
Supporting Information

New cationic Ir(III) complexes without “any soft substituents”: aggregation-induced emission (AIE) and piezochromic luminescence (PCL)

Yue Wang,^a Tianzhi Yang,^a Xingman Liu,^a Guangfu Li,^a Weilong Che,^a Dongxia Zhu*^a and
Zhongmin Su*^a

^a Key Laboratory of Nanobiosensing and Nanobioanalysis at Universities of Jilin Province,
Department of Chemistry, Northeast Normal University, 5268 Renmin Street, Changchun,
Jilin Province 130024, P.R. China *E-mail: zhudx047@nenu.edu.cn, zmsu@nenu.edu.cn

Table of Contents

1. Experimental - general information
2. ¹H NMR spectra of complexes **1** and **2**
3. X-ray crystallographic data
4. Photophysical data
5. Quantum chemical calculations
6. References

1. Experimental - general information

Materials obtained from commercial suppliers were used without further purification. All glassware, syringes, magnetic stirring bars, and needles were thoroughly dried in a convection oven. Reactions were monitored using thin layer chromatography (TLC). Commercial TLC plates were used and the spots were visualized under UV light at 254 and 365 nm. ^1H NMR spectra were performed on a Varian 500 MHz spectrometer with tetramethylsilane (TMS) as the internal standard. Elemental analyses were measured on a Flash EA1112 analyzer. The molecular weights of the two complexes were collected on matrix-assisted laser desorption-ionization time-of-flight (MALDI-TOF) mass spectrometry. The X-ray crystal data of the complexes were recorded by a Bruker Smart Apex II CCD diffractometer with graphite-monochromated Mo $K\alpha$ radiation ($\lambda = 0.71069 \text{ \AA}$). UV-vis absorption spectra were obtained by a Shimadzu UV-3100 spectrophotometer. The emission spectra were recorded by F-7000 FL spectrophotometer. The excited-state lifetime and photoluminescence quantum yields (PLQYs) were measured on using a transient spectrofluorimeter (Edinburgh FLS920). Transmission electron microscopy (TEM) and electron diffraction analyses were recorded by a TECNAI F20 microscope. Powder X-ray diffraction (PXRD) patterns of the different samples were obtained with a Rigaku Dmax 2000. Differential scanning calorimetry (DSC) curves were collected on a NETZSCH thermal analysis DSC200 F₃ under argon with a heating rate $10 \text{ }^\circ\text{C min}^{-1}$.

2. ^1H NMR spectra of complexes 1 and 2

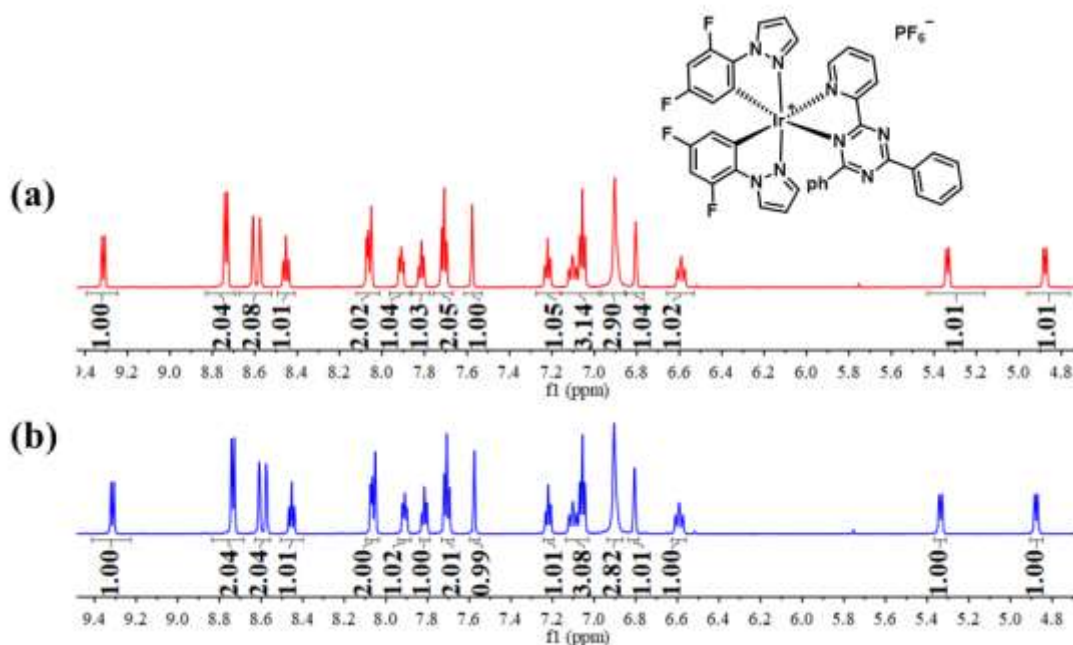


Fig. S1 ^1H NMR spectrum of complex **1** in DMSO-d_6 before grinding (a) and after grinding (b).

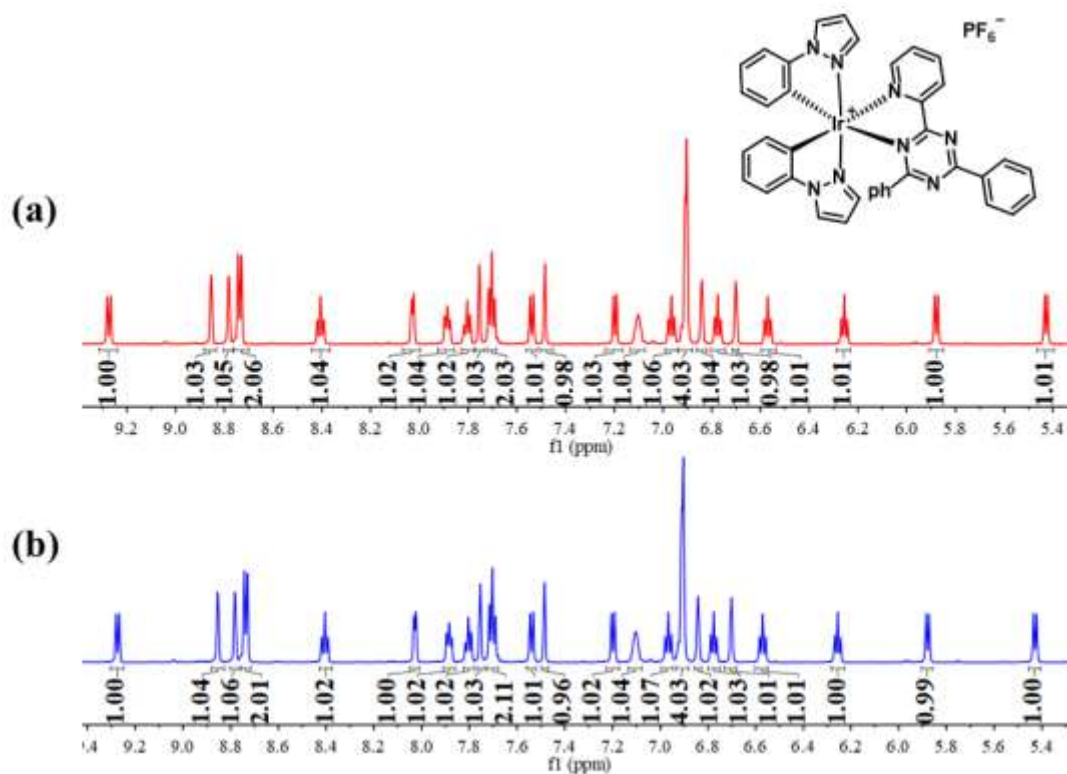


Fig. S2 ^1H NMR spectrum of complex **2** in DMSO-d_6 before grinding (a) and after grinding (b).

3. X-ray crystallographic data

Diffraction data were collected on a Bruker SMART Apex CCD diffractometer using $k(\text{Mo-K})$ radiation ($k = 0.71069 \text{ \AA}$). Cell refinement and data reduction were made by the SAINT program. The structures were determined using the SHELXTL/PC program. The crystallographic data for them have been deposited with the Cambridge Crystallographic Data Centre with CCDC deposition number 1862907 and 1862908. These data can be obtained free of charge from The Cambridge Crystallographic Data Centre via www.ccdc.cam.ac.uk/data_request/cif.

Table S1 Crystal data and structure refinement for complexes **1** and **2**.

	1	2
Empirical formula	$\text{C}_{38}\text{H}_{24}\text{F}_{10}\text{IrN}_8\text{P}$	$\text{C}_{38}\text{H}_{28}\text{F}_6\text{IrN}_8\text{P}$
Formula weight	1005.82	933.85
Temperature (K)	173	153
Crystal system	Orthorhombic	Orthorhombic
space group	Pbca	$\text{P}2_12_12_1$
a / \AA	15.0940(6)	14.458(4)
b / \AA	15.6330(6)	15.043(4)

$c / \text{\AA}$	33.8640(15)	16.466(5)
$\alpha / ^\circ$	90	90
$\beta / ^\circ$	90	90
$\gamma / ^\circ$	90	90
$V / \text{\AA}^3$	7990.7(6)	3581.2(16)
Z	8	4
$\rho_{\text{calc}}(\text{g}/\text{cm}^3)$	1.672	1.732
μ/mm^{-1}	3.467	3.846
R_{int}	0.0557	0.1058
Goodness-of-fit on F^2	1.050	1.059
$R_1^a, wR_2^b [I > 2\sigma(I)]$	0.0265, 0.0652	0.0530, 0.1393
R_1, wR_2 (all data)	0.0384, 0.0698	0.0630, 0.1493

$$^a R_1 = \frac{\sum ||F_o| - |F_c||}{\sum |F_o|}. \quad ^b wR_2 = \left\{ \frac{\sum [w(F_o^2 - F_c^2)^2]}{\sum [w(F_o^2)^2]} \right\}^{1/2}$$

Table S2 Selected bond lengths (Å) for complexes **1** and **2**.

	1	2
Ir1—N3	2.025	2.011
Ir1—C18	2.023	2.035
Ir1—N1	2.016	2.018
Ir1—C9	2.005	2.023
Ir1—N5	2.132	2.166
Ir1—N6	2.195	2.213

4. Photophysical data

Table S3 Photophysical characteristics of complexes **1** and **2**.

	Absorption and emission at room temperature					Emission (77 K)	$k_r \times 10^6 \text{ s}^{-1}$	$k_{nr} \times 10^6 \text{ s}^{-1}$
	$\lambda_{\text{abs}}^a(\text{nm})$	$\lambda_{\text{em}}^a(\text{nm})$	$\lambda_{\text{em}}^b(\text{nm})$	Φ_{em}^b	$\tau^b(\mu\text{s})$	$\lambda_{\text{em}}^c(\text{nm})$		
1	255 (0.416), 291 (0.421)	607	529	0.75	0.67	550	1.12	0.37
2	274 (0.549)	691	578	0.18	0.16	620	1.13	5.13

^aMeasured in CH₃CN (1.0 × 10⁻⁵ M). ^bMeasured in solid state. ^cIn THF glass.

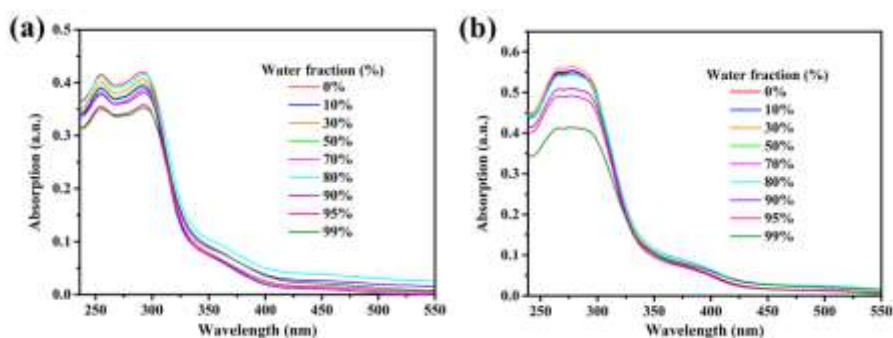


Fig. S3 (a) Absorption spectra of complex **1** (a) and complex **2** (b) in CH₃CN-H₂O mixtures (complex concentration = 1.0×10^{-5} M) with different water fractions (0–99%, v/v) at room temperature.

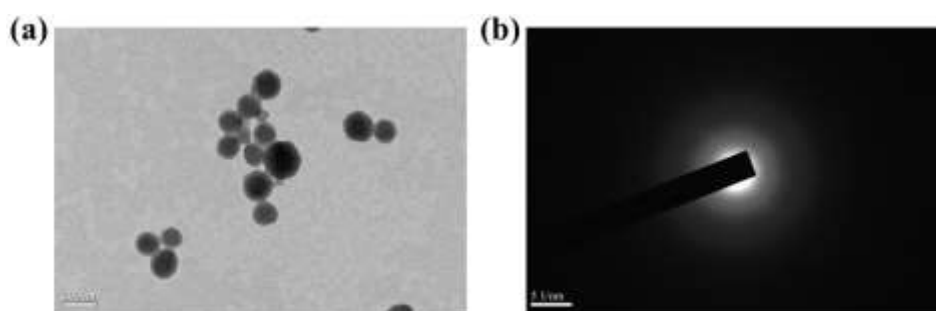


Fig. S4 (a) TEM image of nanoaggregates of complex **1** formed in CH₃CN-H₂O mixtures with 95% water fraction. (b) Electron diffraction pattern of the amorphous nanoaggregates.

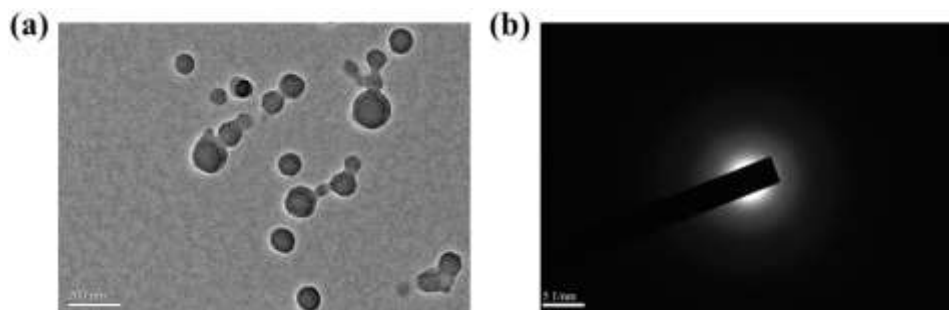


Fig. S5 (a) TEM image of nanoaggregates of complex **2** formed in CH₃CN-H₂O mixtures with 95% water fraction. (b) Electron diffraction pattern of the amorphous nanoaggregates.

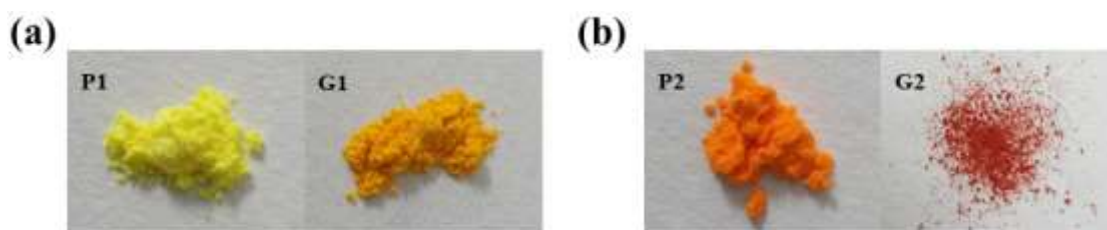


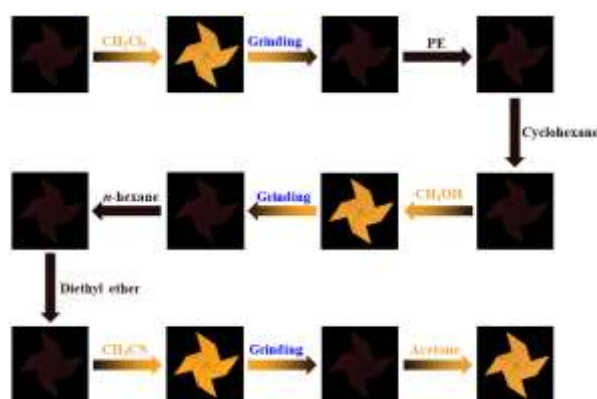
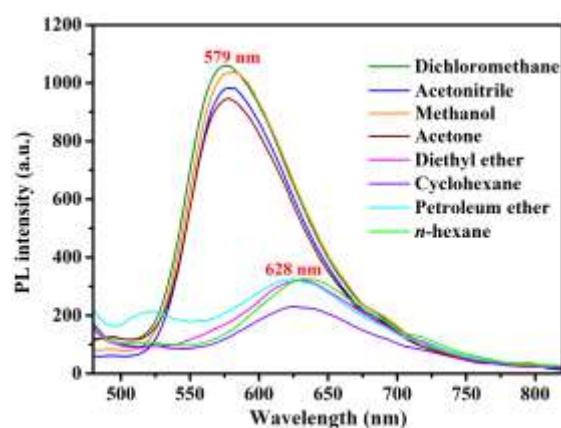
Fig. S6 Image of the corresponding samples in daylight.

Table S4 The Φ_{em} and τ in various states of complex **1**.

	Pristine (P1)	Ground (G1)	CH ₂ Cl ₂ fumed (D1)	Heated (H1)
Φ_{em}	0.75	0.29	0.63	—
$\tau(\mu s)$	0.67	0.25	0.44	—

Table S5 The Φ_{em} and τ in various states of complex **2**.

	Pristine (P2)	Ground (G2)	CH ₂ Cl ₂ fumed (D2)	Heated (H2)
Φ_{em}	0.18	0.03	0.18	0.12
$\tau(\mu s)$	0.16	0.06	0.08	0.08

**Fig. S7** Photographic images under illumination with UV light for the detecting of volatile organic compounds by complex **2** after exposure to different volatile organic compounds and grinding.**Fig. S8** Emission spectra of **G2** after exposure to corresponding solvent (acetone, dichloromethane, methanol, acetonitrile, cyclohexane, petroleum ether, diethyl ether and *n*-hexane).

5. Quantum chemical calculations

All calculations were performed with Gaussian 09 program package.¹ The ground and excited electronic states of complexes were investigated by performing DFT and TD-DFT calculations at the B3LYP level and the PBE0 level, respectively. The 6-31G* basis sets were

employed for optimizing the C, H, N, F atoms, while the Ir atom was described by LANL2DZ basis sets. The calculations on frontier molecular orbital (FMO) properties in the ground state (S_0) and the excited electronic states were carried out after optimization in CH_3CN solution with reference to the crystal data. The solvent effect was taken into account by using the polarisable continuum model (PCM) with acetonitrile as solvent.

Table S6 The calculated energy levels of the lower-lying transitions of complexes **1** and **2**.

Complex	State	eV	f	Assignment (%)	Nature (%)
1	T_1	2.01	0	HOMO \rightarrow LUMO (96.2)	$^3\text{MLCT}$ (19.11)/ $^3\text{LLCT}$ (75.15)
2	T_1	1.80	0	HOMO \rightarrow LUMO (98.1)	$^3\text{MLCT}$ (26.53)/ $^3\text{LLCT}$ (67.89)

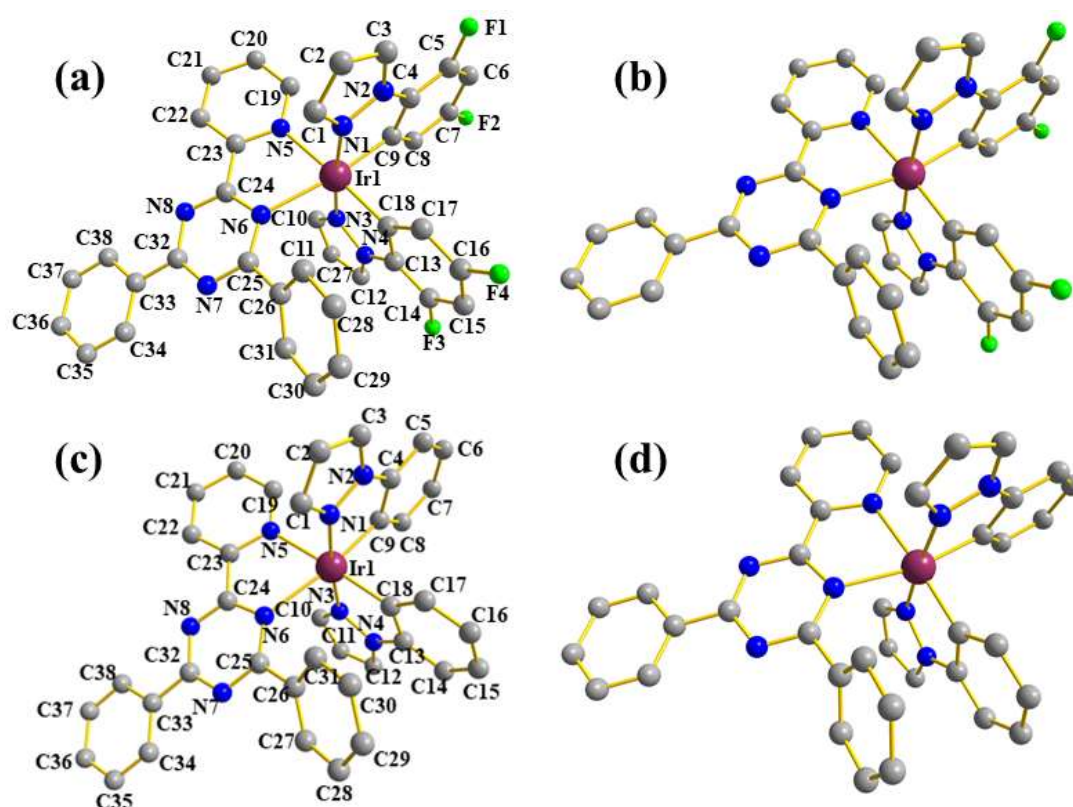


Fig. S9 Optimized geometries of complex **1** at S_0 and T_1 states in CH_3CN solution (a, b), and S_0 and T_1 states for complex **2** (c, d).

Table S7 Selected calculated bond lengths (\AA), bond angles ($^\circ$) and dihedral angles ($^\circ$) at both optimized S_0 and T_1 geometries for complex **1** in acetonitrile solution.

	S_0	T_1
Ir1-N3	2.051	2.051
Ir1-C18	2.036	1.990
Ir1-C9	2.018	2.021
Ir1-N1	2.060	2.054
Ir1-N5	2.193	2.196
Ir1N6	2.316	2.225

C9-Ir1-C18	85.244	90.402
C9-Ir1-N3	95.629	96.540
C18-Ir1-N6	103.076	102.073
N6-Ir1-N3	84.797	87.361
C9-Ir1-N5	96.518	91.436
N6-Ir1-N5	75.097	76.325
C9-Ir1-N6	171.586	167.403
N5-Ir1-C18	175.905	174.111
N1-Ir1-N3	174.419	175.695
C31-C26-C25-N7	37.997	72.526

Table S8 Selected calculated bond lengths (Å), bond angles (°) and dihedral angles (°) at both optimized S_0 and T_1 geometries for complex **2** in acetonitrile solution.

	S_0	T_1
Ir1-N3	2.051	2.052
Ir1-C18	2.039	1.990
Ir1-C9	2.020	2.014
Ir1-N1	2.061	2.059
Ir1-N5	2.199	2.206
Ir1-N6	2.340	2.251
C9-Ir1-C18	85.001	90.941
C9-Ir1-N3	96.008	96.587
C18-Ir1-N6	103.921	102.053
N6-Ir1-N3	84.606	85.752
C9-Ir1-N5	96.331	91.182
N6-Ir1-N5	74.683	75.873
C9-Ir1-N6	170.993	167.006
N5-Ir1-C18	175.877	174.574
N1-Ir1-N3	174.548	175.842
C31-C26-C25-N7	34.687	55.393

6. References

1. M. J. Frisch, G.W. Trucks, H. B. Schlegel, G. E. Scuseria, M. A. Robb, J. R. Cheeseman, G. Scalmani, V. Barone, B. Mennucci, G. A. Petersson, H. Nakatsuji, M. Caricato, X. Li, H. P. Hratchian, A. F. Izmaylov, J. Bloino, G. Zheng, J. L. Sonnenberg, M. Hada, M. Ehara, K. Toyota, R. Fukuda, J. Hasegawa, M. Ishida, T. Nakajima, Y. Honda, O. Kitao, H. Nakai, T. Vreven, J. A. Montgomery, Jr., J. E. Peralta, F. Ogliaro, M. Bearpark, J. J. Heyd, E. Brothers, K. N. Kudin, V. N. Staroverov, R. Kobayashi, J. Normand, K. Raghavachari, A. Rendell, J. C. Burant, S. S. Iyengar, J. Tomasi, M. Cossi, N. Rega, J. M. M. Millam, M. Klene, J. E. K. Knox, J. B. C. Cross, V. Bakken, C. Adamo, J. Jaramillo, R. Gomperts, R. E. Stratmann, O. Yazyev, A. J. Austin, R. Cammi, C. Pomelli, J. W. Ochterski, R. L. Martin, K. Morokuma, V.

G. Zakrzewski, G. A. Voth, P. Salvador, J. J. Dannenberg, S. Dapprich, A. D. Daniels, O. Farkas, J. B. Foresman, J. V. Ortiz, J. Cioslowski and D. J. Fox, Gaussian 09, Revision A.02, Gaussian, Inc, Wallingford CT, **2009**.